

# Computationally guided personalized targeted ablation of persistent atrial fibrillation

Patrick M. Boyle<sup>1,2,3,4,8</sup>, Tarek Zghaib<sup>5,8</sup>, Sohail Zahid<sup>1</sup>, Rheeda L. Ali<sup>2</sup>, Dongdong Deng<sup>2</sup>, William H. Franceschi<sup>1</sup>, Joe B. Hakim<sup>2</sup>, Michael J. Murphy<sup>1</sup>, Adityo Prakosa<sup>2</sup>, Stefan L. Zimmerman<sup>6</sup>, Hiroshi Ashikaga<sup>5</sup>, Joseph E. Marine<sup>5</sup>, Aravindan Kolandaivelu<sup>5</sup>, Saman Nazarian<sup>7</sup>, David D. Spragg<sup>5</sup>, Hugh Calkins<sup>5</sup> and Natalia A. Trayanova<sup>1,2\*</sup>

**Atrial fibrillation (AF)—the most common arrhythmia—significantly increases the risk of stroke and heart failure. Although catheter ablation can restore normal heart rhythms, patients with persistent AF who develop atrial fibrosis often undergo multiple failed ablations, and thus increased procedural risks. Here, we present personalized computational modelling for the reliable predetermination of ablation targets, which are then used to guide the ablation procedure in patients with persistent AF and atrial fibrosis. First, we show that a computational model of the atria of patients identifies fibrotic tissue that, if ablated, will not sustain AF. Then, we report the results of integrating the target ablation sites in a clinical mapping system and testing its feasibility in ten patients with persistent AF. The computational prediction of ablation targets avoids lengthy electrical mapping and could improve the accuracy and efficacy of targeted AF ablation in patients while eliminating the need for repeat procedures.**

With a prevalence of 1–2% worldwide, atrial fibrillation (AF)—an abnormal uncoordinated rhythm in the upper chambers of the heart—is the most common cardiac rhythm disorder, and a major contributor to mortality and morbidity<sup>1</sup>. Its burden on the health care system is expected to follow a projected increase in AF prevalence over the coming decades<sup>2</sup>. Patients afflicted by AF have a higher mortality rate due to a dramatically increased risk of stroke<sup>1</sup>. AF is also associated with diminished quality of life<sup>3</sup>, increased rates of cognitive impairment<sup>4</sup> and high treatment costs<sup>5</sup>. Aiming to achieve a permanent cure for AF, catheter-based radiofrequency ablation uses a catheter inserted into the heart to deliver energy and destroy the ability of cardiac tissue to conduct electrical signals, thus terminating the arrhythmia. The standard-of-care ablation treatment for AF is pulmonary vein isolation (PVI), which encircles the pulmonary veins with lesions, preventing abnormal electric signals generated in the veins from invading the atria<sup>6</sup>.

However, in patients with the persistent form of AF (PsAF), who typically develop fibrotic remodelling in the atria<sup>7–10</sup>, the mechanisms giving rise to AF shift from electrical abnormality in the pulmonary veins to re-circulating electrical waves perpetuated by the fibrotic substrate<sup>11</sup>. In these patients with PsAF, all attempts to target the arrhythmogenic sources in the fibrotic substrate, such as execution of linear ablation lesions across the left atrial roof and mitral valve isthmus, and ablations of complex fractionated atrial electrograms, have failed to deliver reasonable outcomes<sup>12</sup>, as these approaches do not incorporate strategies for finding the appropriate ablation targets in the atrial substrate on the basis of AF mechanisms. Furthermore, these are all ‘one-size-fits-all’ ablation approaches to treat a disease characterized by high interindividual

variability in fibrosis distribution and, consequently, in the sources that sustain AF<sup>11</sup>. As a result, patients with PsAF undergo multiple failed ablations with increasing procedural risks. For these patients, there is currently no reliable AF ablation option. Developing and implementing new approaches in clinical practice for the ablation of patients with PsAF and atrial fibrosis, where the patient-specific AF ablation targets in the fibrotic substrate are determined accurately and reliably, will result in an effective antiarrhythmia treatment, and will spare these patients from increasingly complex repeat procedures, reducing morbidity.

Here, we present the proof of concept of a technology for targeted ablation of patients with PsAF and atrial fibrosis, where reliable and optimal ablation targets are determined non-invasively via personalized pre-procedure computational modelling and utilized to steer patient treatment. We term this approach optimal target identification via modelling of arrhythmogenesis (OPTIMA). The personalized computational models of the atria are reconstructed from each individual patient's late gadolinium enhancement magnetic resonance imaging (LGE-MRI) scans. The prediction of the ablation targets in the fibrotic substrate is thus custom-tailored to each patient. Furthermore, as the targets are calculated offline before the clinical procedure, the approach avoids lengthy invasive mapping of the patient's atrial electrical activity. Importantly, the methodology involves a fundamentally new concept: it is designed to completely eliminate the ability of the patient's fibrotic substrate to sustain AF. This ablation concept is radically different from any existing AF ablation strategies, as we aim to eliminate not only the clinically manifested AF, but also latent atrial arrhythmias that could arise from the fibrotic substrate, including those that might emerge following initial ablation. The prospect of uncovering all

<sup>1</sup>Department of Biomedical Engineering, Johns Hopkins University, Baltimore, MD, USA. <sup>2</sup>Institute for Computational Medicine, Johns Hopkins University, Baltimore, MD, USA. <sup>3</sup>Department of Bioengineering, University of Washington, Seattle, WA, USA. <sup>4</sup>Institute for Stem Cell and Regenerative Medicine, University of Washington, Seattle, WA, USA. <sup>5</sup>Division of Cardiology, Johns Hopkins University School of Medicine, Baltimore, MD, USA. <sup>6</sup>Department of Radiology and Radiological Sciences, Johns Hopkins University School of Medicine, Baltimore, MD, USA. <sup>7</sup>Division of Cardiology, Perelman School of Medicine, University of Pennsylvania, Philadelphia, PA, USA. <sup>8</sup>These authors contributed equally: Patrick M. Boyle, Tarek Zghaib. \*e-mail: [ntrayanova@jhu.edu](mailto:ntrayanova@jhu.edu)

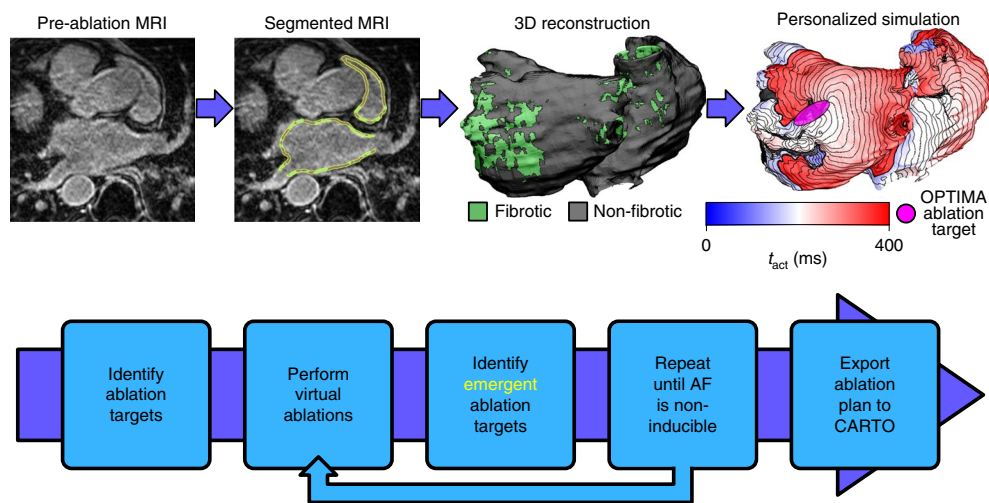


**Fig. 1 | OPTIMA approach flowchart.** Top: overview of the approach. LGE-MRI scans for each patient with PsAF are processed to reconstruct a personalized 3D model of the patient's fibrotic atria. Personalized simulations are then conducted to determine all of the arrhythmias that could arise in the fibrotic substrate, and the custom-tailored OPTIMA ablation targets are determined.  $t_{act}$ , activation time. Bottom: detailed steps undertaken to find the OPTIMA ablation targets based on the arrhythmias that arise in the atrial fibrotic substrate following rapid pacing from 40 uniformly distributed bi-atrial sites. From the analysis of the pacing-induced arrhythmias, an initial set of lesions is determined, consisting of the locations of the persistent RDs and ablation lines connecting these sites to the closest non-conductive anatomical barriers (pulmonary vein ostia, superior/inferior vena cava openings or mitral/tricuspid valve annuli). Virtual ablation of these targets is performed next, where the lesions are rendered non-conductive in the model. The rapid pacing protocol is then repeated to determine whether new arrhythmias arise in the post-ablation substrate. The latter two steps are repeated until AF can no longer be induced in the patient's atrial model. Finally, the personalized ablation treatment plan is exported to a format compatible with the clinical electroanatomic navigation system (that is, CARTO).

of the potential sources of AF in the patient-specific fibrotic substrate—and not only those that sustain the clinical AF episode—is unique to our personalized modelling prediction of ablation targets. OPTIMA is thus designed not only to make ablation efficacious in patients with PsAF, but also to potentially eliminate the need for repeat ablations.

The feasibility of the OPTIMA approach to guide ablation in patients with PsAF was shown in a prospective clinical study ( $n=10$ ). The success of this feasibility study could open the door to means of delivering treatment to patients with PsAF, and thus chart a pathway for the personalized management of atrial arrhythmia.

### The OPTIMA methodology

A flow chart of the processes that comprise OPTIMA is illustrated in Fig. 1. The top row of Fig. 1 presents an overview of the approach. For each patient with PsAF, a personalized three-dimensional (3D) atrial geometric model is reconstructed from the segmented LGE-MRI before the ablation procedure, with representations of both fibrotic and non-fibrotic tissue. Region-specific cell and tissue electrical properties are then assigned to the geometric model. Next, personalized simulations are conducted to determine all of the atrial arrhythmias that could arise from the fibrotic substrate; this is done by analysing model responses following rapid pacing from 40 uniformly distributed bi-atrial sites. On the basis of the model responses, an optimal (minimum-size) set of ablation lesions is determined that fully eliminates the arrhythmogenic propensity of the atrial substrate. These are the OPTIMA ablation targets.

The bottom row of Fig. 1 illustrates the steps undertaken in finding the OPTIMA ablation targets. Analysing the pacing-induced arrhythmias, persistent re-entrant drivers (RDs) sustaining AF, as well as macro re-entrant atrial tachycardias or flutters, are determined. The initial set of ablation lesions constitutes the locations of these RDs and, if necessary, ablation lines transecting any macro re-entrant pathways. This set of virtual lesions is then implemented in the model and multisite pacing is repeated to determine whether

the lesions render the fibrotic substrate fully non-inducible for atrial arrhythmias. Should new arrhythmias emerge post-virtual ablation (RDs, or macro re-entrant atrial tachycardias or flutters), the additional targets are determined, and the entire protocol is repeated until complete elimination of the fibrotic substrate's ability to sustain arrhythmias is achieved. This represents the hallmark of our approach. In cases where the targets are close to a nearby non-conductive anatomical barrier, they are connected to that barrier via a shortest-distance linear lesion to prevent the formation of macro re-entrant atrial tachycardias or flutters<sup>13</sup>. This completes the generation of the personalized OPTIMA ablation target set.

Supplementary Video 1 presents a dynamic illustration of all OPTIMA steps. A full description of the OPTIMA methodology, including detail about the simulation procedure, arrhythmia induction and analysis, and ablation targets, is provided in the Methods.

### Proof-of-concept clinical feasibility study

A proof-of-concept prospective clinical study to demonstrate the feasibility of our technology to guide patient treatment was conducted in ten patients with PsAF and atrial fibrotic remodelling. Patients were referred for OPTIMA-guided catheter ablation and underwent pre-ablation LGE-MRI. Patient recruitment and characteristics are described in Supplementary Table 1. The majority of our patients with PsAF (60%) had previously failed catheter ablation procedures (up to three previous ablations), and most of them had co-morbidities (for example, a median (interquartile range) CHA<sub>2</sub>DS<sub>2</sub>-VASC score of 2 (1–2), a mean age of  $66 \pm 7$  years and a mean body mass index of  $30 \pm 5$  kg m<sup>-2</sup>).

On the day of the clinical procedure, the custom-tailored OPTIMA targets were loaded into the electroanatomic navigation system in a stepwise process (Fig. 2). This involved segmenting the patient's left atrial geometry from the magnetic resonance angiography (MRA) scan to construct a 3D surface mesh. Unlike LGE-MRI, the MRA surface shell provides visualization of the pulmonary veins, left atrial appendage and left lateral ridge needed for

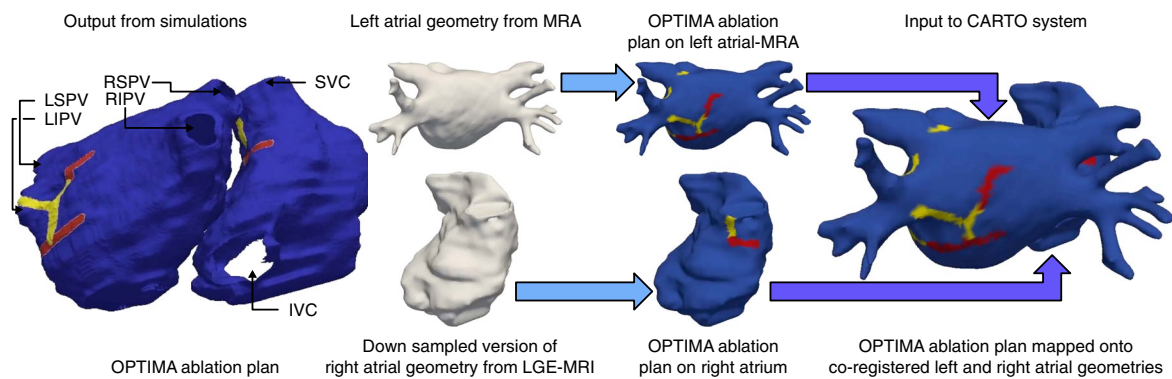


**Fig. 2 | Schematic summarizing the process of importing OPTIMA ablation targets into CARTO.** The starting point for this process is the set of outputs from the OPTIMA approach (that is, ablation targets on bi-atrial volumetric mesh reconstructed from LGE-MRI). Red regions indicate ablation targets from the analysis, while yellow regions indicate connecting lines. Targets located in the left atrium are mapped via co-registration onto a geometric reconstruction of the left atrial endocardial surface extracted from the same patient's MRA scan, which includes the anatomical features needed for periprocedural registration (for example, the prominent ridge between the left pulmonary veins and lateral left atrium). Notably, the left atrial geometry from MRA is a surface mesh (that is, a two-dimensional manifold in 3D space) and not a volumetric mesh. Since right atrial segmentation from the MRA scan is not possible, we instead derive a surface mesh of the right atrial endocardium, including any ablation targets, from the LGE-MRI-based model. The right atrial surface mesh with ablation targets is then downsampled, since high-resolution meshes cannot be loaded into the clinical mapping system. Finally, the left atrial MRA and downsampled right atrial surface meshes with the OPTIMA ablation plan are aligned and scale-matched via affine transformation, resulting in a geometric model ready to be converted into a Visualization Toolkit file suitable for importation into the CARTO system. IVC, inferior vena cava; LIPV, left inferior pulmonary vein; LSPV, left superior pulmonary vein; RIPV, right inferior pulmonary vein; RSPV, right superior pulmonary vein; SVC, superior vena cava.

navigation during the procedure. Next, OPTIMA ablation targets in the left atrium were co-registered with the MRA surface shell. The right atrial surface shell was also co-registered, using affine transformation, with the left atrial MRA reference shell. Finally, the left and right atrial surface shells with the OPTIMA targets were loaded into the electroanatomical navigation system and displayed in real time, ready to guide the ablation procedure. A full description of the same-day pre-procedure steps outlined above is provided in the Methods. During the procedure, the ablation catheter was steered directly towards the OPTIMA targets without previous mapping. The targets were ablated sequentially.

The pre-procedure for determination of the OPTIMA targets is illustrated in Fig. 3 for three patients from the ten-patient cohort. Presented are the activation sequences during AF and those emerging following the first set of virtual ablations, as well as the final custom-tailored OPTIMA ablation treatment plans (see also Supplementary Videos 2–4). The results for another three patients are presented in Supplementary Fig. 1. Overall, the first execution of the multisite pacing protocol resulted in 4.5 (2.3–6.0) RDs per model. In one patient (patient 4), the analysis found no RDs or atrial flutters; accordingly, no OPTIMA-guided ablation was performed. Post-virtual ablation, emergent RDs were observed in three patient-specific models (between one and five RDs), at locations distinct from those of RDs in the original models. The most common locations of the RDs, including the emergent ones, were the posterior left atrial wall (17%) and the left pulmonary veins (19%). The combined results of OPTIMA analysis regarding the RDs in all ten patients are summarized in Table 1. Supplementary Table 2 details comprehensively the number and location of all RDs, as well as the number of pacing sites from which a given RD was induced. As shown by the data from the OPTIMA analysis presented in Table 1 and Supplementary Table 2, the right atrium could also sustain RDs, including emergent ones. This is consistent with the fact that the right atria in the ten-patient cohort displayed significant fibrotic remodelling of a degree comparable to that of the left atria ( $18.6 \pm 14.2$  versus  $24.1 \pm 12.4\%$ ; Supplementary Table 1). The total number of RDs (including emergent ones) in the RAs of all patients was 12, while the total number of left atrial RDs was 32, confirm-

ing the higher level of arrhythmogenic propensity in the left atrium, consistent with previous findings<sup>14,15</sup>.

Procedural clinical data from OPTIMA-driven ablation in our feasibility study are presented in Fig. 4 for three patients. Illustrated are the locations of left atrial ablation lesions at the end of the procedure, as rendered in the electroanatomic mapping system, and intracardiac electrograms during the procedure. Additional clinical data for two patients are presented in Supplementary Fig. 2. As the right atrium is typically not ablated during a routine procedure in patients with PsAF, and because this study aimed only to demonstrate the feasibility of the OPTIMA approach, physicians' practice played a role; physicians thus sometimes elected to not ablate targets in the right atrium. Specifically, while 97% of all targets in left atria were ablated (2.5 (2–4) per patient), only 58% of right atrial targets were ablated (Table 1 and Supplementary Table 2). Only one left atrial target in all ten patients was not ablated for safety reasons, due to its proximity to the His bundle. Post-ablation, patients were followed prospectively; the follow-up period was 309 (245–386) days. Ablation outcomes data are presented in Supplementary Table 3.

Conducting this prospective clinical study showed the feasibility of our OPTIMA approach in guiding treatment in patients with PsAF and fibrosis.

## Discussion

We have introduced a technology for the targeted ablation of patients with PsAF and atrial fibrosis, and demonstrated the feasibility of this technology to guide patient treatment in a prospective study of ten patients. This is a clinical application of an approach that uses simulations conducted in computational models, including patient-specific fibrosis and atrial geometry, to construct specific and detailed ablation plans for each individual.

We used state-of-the-art multi-scale computational modelling to determine non-invasively the optimal set of patient-tailored targets for catheter ablation of the fibrotic atrial substrate. The targets were then incorporated into the clinical procedure and used to steer patient treatment. By linking the spatial scales, from the cell to the patient atrium, the computational prediction of PsAF ablation targets is informed by deep mechanistic understanding<sup>16–18</sup> of how AF



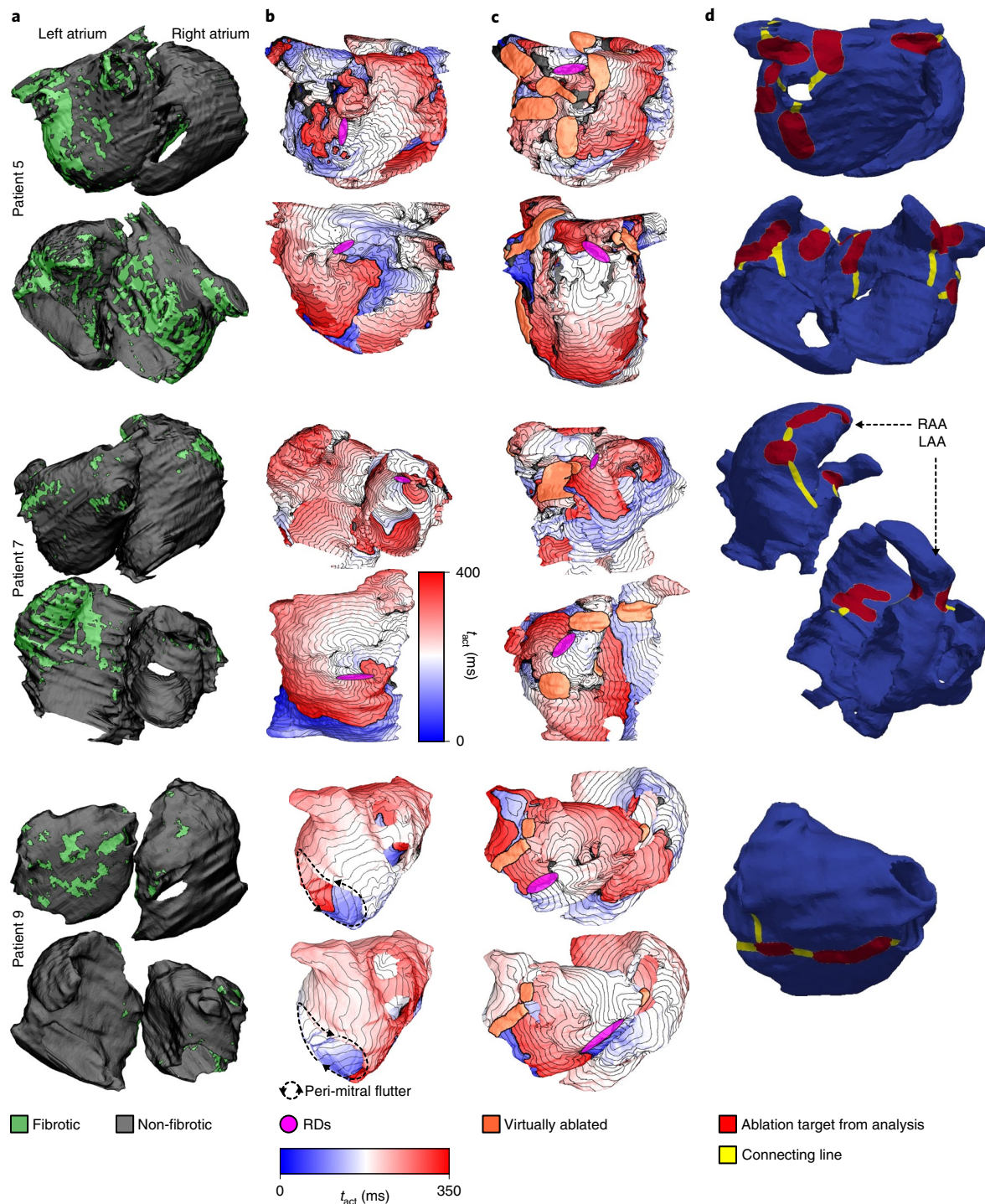


**Fig. 3 | Examples of the process to determine the OPTIMA ablation targets for three patients.** Patient 5 is a 68-year-old man with one previous failed ablation (see also Supplementary Video 2). Patient 7 is a 49-year-old man with one previous failed ablation (see also Supplementary Video 3). Patient 9 is a 72-year-old man with two previous failed ablations (see also Supplementary Video 4). **a**, Posterior (top) and anterior (bottom) views of the three patient-specific atrial models as reconstructed from segmented LGE-MRI scans, including the distribution of fibrotic tissue. **b**, Two examples per model of arrhythmia activation sequences induced by the rapid pacing protocol, and the corresponding persistent RDs (pink) obtained from analysis of the induced arrhythmias. For patient 9, no RD-perpetuated AF was observed following the initial pacing protocol. However, peri-mitral macro re-entrant tachycardia was found, and transient episodes of non-sustained re-entry were documented in two locations on the posterior left atrium. All activation maps share the same time scale except the lower panel activation map for patient 7. **c**, Two examples per model of activation sequences associated with arrhythmia emerging anew in the models following virtual ablation (lesions shown in orange), and the corresponding emergent RDs. For patient 9, following virtual ablation to render the initiation of peri-mitral re-entry impossible, stable emergent RDs were observed in the same two locations where non-sustained re-entries were observed following the initial rapid pacing. **d**, Custom-tailored OPTIMA ablation treatment plans, including targets corresponding to all RDs (pre-ablation and emergent) and lesion lines connecting these target RDs to non-conductive tissue boundaries. LAA, left atrial appendage; RAA, right atrial appendage.

**Table 1 | Summary of OPTIMA ablation data in all ten patients**

ID	Total model RDs (including the LAA and RAA)	OPTIMA left atrial RDs	OPTIMA right atrial RDs	Left atrial targets ablated	Right atrial targets ablated
1	6	4	1 <sup>a</sup>	4	1
2	1	0	1	0	1
3	8	5 <sup>a</sup>	1 <sup>a</sup>	5	1
5	14	9 <sup>a</sup>	2 <sup>b</sup>	9	0
6	4	2	1 <sup>a</sup>	2	0
7	7	2	4 <sup>a</sup>	2	4
8	6	5	1	4	0
9	2	2	0	2	0
10	5	3 <sup>a</sup>	1	3	0
<b>Total</b>	<b>53</b>	<b>32</b>	<b>12</b>	<b>31 (97%)</b>	<b>7 (58%)</b>
<b>Summary</b>	<b>5.5 (2.50–6.75)</b>	<b>2.5 (2.00–4.75)</b>	<b>1 (1–1)</b>	<b>2.5 (2–4)</b>	<b>0 (0–1)</b>

Summary measures are displayed as medians (interquartile ranges). Of the RDs predicted by modelling, those found in the left atrial appendage (LAA) or right atrial appendage (RAA) were not part of the OPTIMA ablation target set imported into CARTO (see Methods), as LAA and RAA ablation is not recommended due to the high risk of stroke. Thus, the total number of model RDs is different from the total number of RD targets in the OPTIMA set. <sup>a</sup>Model RDs in the LAA or RAA excluded from the OPTIMA set. <sup>b</sup>Multiple model RDs in the LAA or RAA.

dynamics are modulated by the patient-specific fibrotic substrate. OPTIMA-guided ablation embodies the incorporation of cutting-edge biomedical and computational engineering in solving complex clinical challenges in cardiovascular medicine. While there has been another attempt to use personalized computational simulations to guide clinical ablation of AF in patients<sup>19</sup>, it involved simulating—on the endocardial computed tomography-based left atrial shell only—a few different template ablation strategies (for example, PVI only, PVI plus lines, and so on) and empirically selecting the best-performing one to be executed clinically, following the inspection of simulation results. In contrast, the 3D bi-atrial OPTIMA approach targets—in a personalized manner—the RD-sustaining properties of the fibrotic substrate, including those that appear following an initial round of virtual ablations, and is fully integrated in the clinical workflow via co-registration with the electroanatomical mapping system.

The OPTIMA approach does not use patient-specific electrophysiological parameters in the models; the personalized aspects in the models involve patient-specific atrial geometry and fibrosis distribution. In the current state of the art, personalization of electrophysiological parameters would necessitate invasive data acquisition in each patient. We deliberately avoided this in the design of the OPTIMA approach, since non-invasive target assessment is an advantage of our approach. Interpatient variability in electrophysiology could affect ablation target location predictions<sup>20</sup>; however, the potential uncertainty in target locations due to the use of average human PsAF electrophysiology is significantly alleviated by the use of virtual ablations and repeated AF inducibility protocols in the models, as we have previously demonstrated<sup>21</sup>. Future advancements in OPTIMA could potentially achieve a more advanced and accurate personalization of the atrial models.

Current AF mapping techniques rely on invasive intracardiac manoeuvring of a catheter to hundreds of atrial locations, to record (often sequentially and manually) the underlying electrogram characteristics at each site, so that the ablation targets can be determined. Recently, ablation strategies that rely on finding and subsequently targeting substrate RDs have also emerged. These include focal impulse and rotor modulation<sup>22</sup> and non-invasive electrocar-

diographic imaging (ECGI)<sup>23</sup>. These RD-guided ablation strategies only target RDs that currently manifest in a patient's clinical or induced AF episodes; however, new RDs could arise in the fibrotic substrate after it is modified by the initial set of ablation lesions, leading to AF recurrence<sup>24–26</sup>.

The OPTIMA strategy is radically different: it is designed to target all possible RDs, including those that could emerge if the arrhythmia-sustaining propensity of the fibrotic substrate is not eliminated by the initial ablation. When needed, we also incorporate short linear ablations connecting targeted RD sites with the nearest non-conductive anatomical obstacle to prevent macro re-entrant waves from circumnavigating RD ablation lesions, thus decreasing the probability of emergent atrial tachycardias/flutter and arrhythmia recurrence. In its design, the OPTIMA approach represents the most comprehensive PsAF treatment strategy because of its potential to eradicate the ability of the patient's fibrotic substrate to sustain AF, which eliminates the need for repeat ablations. Uncovering all of the potential sources of AF in the patient-specific fibrotic substrate—and not only those that sustain the clinically presenting AF episode—is unique to the computationally driven OPTIMA approach.

Clinical imaging and OPTIMA simulations revealed that in patients with PsAF the right atrium could also develop fibrotic remodelling and sustain RDs, which could then be targeted for ablation. This underscores the importance of a comprehensive evaluation and targeting of the fibrotic substrate at first ablation in the effort to decrease and even eliminate repeat ablations of increasing difficulty, which often result in increased morbidity.

As part of the assessment of the feasibility of this technology, we developed an approach to import the OPTIMA targets into the clinical electroanatomical mapping system. Furthermore, the integration of computational heart modelling into the clinical procedure was achieved here within the clinical workflow and timeline. The personalized OPTIMA targets were calculated offline before ablation, with all OPTIMA steps being completed within 2.5–5 d based on patient LGE-MRI scans acquired 3–5 d before the clinical procedure. Importation of the OPTIMA targets into the clinical mapping system was done immediately before onset of the procedure, allowing the ablation catheter to be directly navigated to the displayed OPTIMA targets. Thus, our non-invasive approach could provide not only a reliable and accurate prediction of AF ablation targets, but could also avoid time-consuming and difficult mapping of atrial electrical activity.

As this is a proof-of-concept feasibility study of a technology, and not a clinical trial, it was inherently not designed to evaluate procedural outcomes and there was no way to account for the fact that some of the targets in the right atrium were not ablated. Nonetheless, PsAF did not recur in any of the patients, and only one patient underwent paroxysmal AF/atrial flutter ablation during the follow-up period (patient 3; Supplementary Table 3). Additionally, 44% of patients (four out of nine) remained on antiarrhythmic drugs. Patient 3 was of very low clinical expectation pre-procedure since he had had the most previous ablations (three), the largest amount of left atrial fibrosis (46.9%), the largest left and right atrial volume indices (87.8 and 74.4 ml m<sup>-2</sup>, respectively), and the worst CHA<sub>2</sub>DS<sub>2</sub>-VASc score (5). We view the clinical outcomes here as being considerably better than the standard-of-care AF ablation in patients with PsAF, the success rate of which is ~50%<sup>27</sup>, although quantitative comparisons cannot be made. To establish the efficacy of the OPTIMA approach in AF suppression in the population of patients with PsAF with fibrotic remodelling, a clinical trial with an adequate sample size and randomized comparisons will need to be undertaken.

## Outlook

Should the OPTIMA approach prove beneficial in a randomized clinical study, it could then transform the management of patients

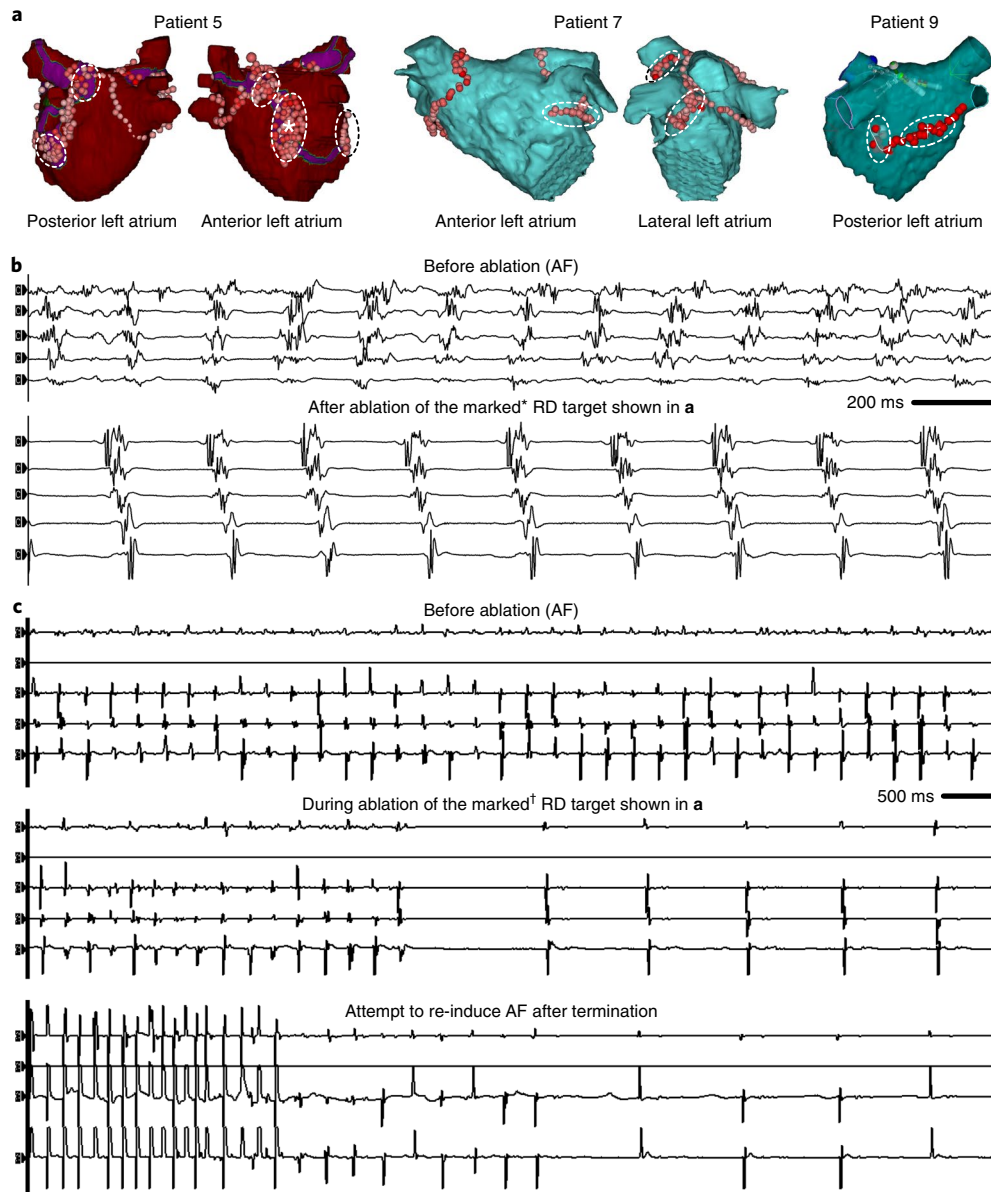


**Fig. 4 | Data from the OPTIMA-driven ablation procedures in the three patients from Fig. 2. a**, Sites of ablation delivery (with catheter tip locations marked by red dots) in the left atrium, as rendered by the CARTO intracardiac mapping system at the end of the clinical ablation procedure in three patients. Dashed ellipses indicate the locations ablated based on the locations of persistent RDs, as identified by OPTIMA. Asterisks indicate marked RD targets. As patient 7 also had targets in the right atrium, Supplementary Fig. 3 shows the annotated right atrial CARTO map from the same procedure. **b,c**, Bipolar electrogram recordings from a decapolar catheter placed in the coronary sinus of patient 5 (**b**) and patient 9 (**c**) during the procedure. The sets of five recordings are from the proximal (top) to distal leads (bottom). In patient 5, ablation of the marked anterior left atrial RD target (shown in **a** by an asterisk for patient 5) resulted in a transient change from AF (top set of five electrograms in **b**) to an organized atrial tachycardia or flutter (bottom set of five electrograms in **b**). For patient 9, the top set of electrograms show stable induced AF pre-ablation. This was terminated abruptly (middle set of five electrograms in **c**) on ablation of the marked posterior left atrial target (shown in **a** by a dagger for patient 9), and AF could not be re-induced despite aggressive rapid pacing (bottom set of five electrograms in **c**).

with PsAF and fibrosis—a population for whom there is currently no reliable AF ablation option. The ability to non-invasively determine the personalized optimal ablation targets in silico before the procedure could spare patients from prolonged intracardiac mapping to probe for potential ablation targets, increased radiation exposure and potentially arrhythmogenic ablation lesions. If successfully implemented in clinical practice, this approach could be a significant step towards achieving long-term freedom from PsAF while also making ablation procedures more precise and less time consuming. Finally, our study underscores the potential utility of

computational and data-driven approaches in cardiac patient care, and exemplifies the trend of merging engineering and medicine towards improving health care.

## Methods

**Patient recruitment.** Ten patients with symptomatic, drug-refractory PsAF who presented to Johns Hopkins Hospital for catheter ablation were included in this prospective study and underwent OPTIMA-guided ablation. All patients provided written informed consent, under a protocol approved by the Johns Hopkins Institutional Review Board, for both the ablation procedure and inclusion in medical research at the time of the procedure. Exclusion criteria included: patients



with cardiac devices such as pacemakers and internal cardiac defibrillators, and with acute or chronic renal insufficiency (glomerular filtration rate  $< 30 \text{ ml min}^{-1}$  per  $1.73 \text{ m}^2$ ); patients who were unable to adhere to the follow-up protocol; patients with contraindication to MRI, including ferromagnetic aneurysm clips, metal in the eye, and implanted ferromagnetic or other MRI-incompatible devices; and patients with a history of allergic reactions to gadolinium-based contrast agents. Supplementary Table 1 summarizes patients' clinical characteristics. The mean age was  $66.1 \pm 8.0$  years, the mean body mass index was  $29 \pm 4 \text{ kg m}^{-2}$ , and nine out of ten patients (90%) were men. Six out of ten cases (60%) were repeat ablations, with one patient undergoing his fourth AF ablation. In three out of six patients who were undergoing repeat ablations, at least one reconnected pulmonary vein was observed at the time of the OPTIMA-guided procedure.

**MRI acquisition.** Images were obtained using a 1.5 Tesla MRI scanner (Avanto; Siemens) and a six-channel phased-array body coil in combination with a six-channel spine matrix coil. Contrast-enhanced 3D time-resolved MRA (TWIST; Siemens), obtained immediately following intravenous administration of  $0.1 \text{ mmol kg}^{-1}$  contrast, was used to define the left atrium and pulmonary vein anatomy (echo time: 1.1 ms; repetition time: 2.5 ms; in-plane resolution:  $0.7 \text{ mm} \times 0.7 \text{ mm}$ ; slice thickness: 1.5 mm). To optimize the image quality, patients with PsAF were kept on antiarrhythmic medications and/or referred for cardioversion before MRI. The MRI examination was performed using the same methodology, regardless of the presenting rhythm. In individuals with AF, correlations have been shown between areas of high LGE and fibrotic regions in the myocardium, as identified histologically<sup>28</sup> or via intracardiac mapping<sup>29</sup>.

LGE-MRI scans were acquired within a range of 15–25 (mean:  $18.8 \pm 2.4$ ) minutes (following  $0.2 \text{ mmol kg}^{-1}$  gadolinium injection (gadopentetate dimeglumine; Bayer Healthcare Pharmaceuticals) using a fat-saturated 3D inversion recovery-prepared fast spoiled gradient-recalled echo sequence with respiratory navigation and electrocardiogram gating), an echo time of 1.52 ms, a repetition time of 3.8 ms, an in-plane resolution of  $1.3 \times 1.3$ , a slice thickness of 2.5 mm and a flip angle of  $10^\circ$ . The trigger time for 3D LGE-MRI images was optimized to acquire imaging data during diastole of the left atrium, as dictated by inspection of the cine images. The optimal inversion time was identified with a TI scout scan (median: 270 ms; range: 240–290 ms), to maximize nulling of the left ventricular myocardium.

**Image processing to construct a personalized geometric model of the of patient atrium.** A full description of the geometric model reconstruction methodology can be found in our previous publications<sup>17,18</sup>. Briefly, epicardial and endocardial contours of the left and right atria were manually delineated using the ITK-SNAP software package<sup>30</sup>. For pixels in the transmural space between contours in each slice, fibrotic and non-fibrotic tissue regions were differentiated using the image intensity ratio (IIR)-based approach<sup>29</sup>. The IIR of each atrial wall voxel was calculated by normalizing its LGE-MRI signal intensity to the mean intensity of the left atrial blood pool. Voxels with an IIR of  $> 1.22$  were classified as fibrotic; we have previously shown that regions with this property correlate to low-voltage areas observed during intracardiac mapping<sup>29</sup>. The IIR approach used here has been specifically designed to mitigate the uncertainty in threshold-based methods in segmenting LGE-MRI scans<sup>31</sup> since it uses ratiometric values instead of raw voxel intensities<sup>29</sup>.

Shape-based interpolation<sup>32</sup> was used to up-sample segmented images to an isotropic voxel size of  $400 \mu\text{m}^3$ . Next, high-resolution tetrahedral meshes were generated using an established automated approach<sup>33</sup>. These volumetric meshes were 3D, and included atrial wall thickness and the 3D distribution of fibrotic remodelling reconstructed from LGE-MRI. Across all ten finite-element atrial meshes, the average element edge length was  $428.4 \pm 24.3 \mu\text{m}$  and the number of nodes ranged from  $\sim 1$  million to  $\sim 2.6$  million. These mesh characteristics are consistent with those reported in previous studies as appropriate for conducting electrophysiological simulations<sup>34,35</sup>. For each atrial model, realistic myocardial fibre orientations were estimated using a diffeomorphic mapping technique to transform the relevant conductivity tensors from the geometry of an atlas mesh into the patient-specific geometry reconstructed from LGE-MRI, as we have previously described<sup>16,33,36–38</sup>. Volume indices for both atria were obtained by dividing the cavity volume (extracted from each patient-specific model) by body surface area.

In our 3D models, the electrical connection between the right and left atrium was the interatrial septum, since the structure and connectivity of interatrial conduction pathways (for example, Bachmann's bundle) cannot be recovered from LGE-MRI scans. Although rule-based methods have been used to impose bundle structures in computational models of atria<sup>39</sup>, we opted not to use this type of approach since we did not want to jeopardize the feasibility of the OPTIMA process being part of the clinical workflow by adding considerable complexity to the model construction stage. Moreover, while the inclusion of complex intra-atrial structures may change the particular ways by which paced activity devolves into episodes of arrhythmia, it would not be expected to change the specific RD anchoring locations, which are predominantly influenced by the patient-specific pattern of structural remodelling<sup>16–18</sup>.

#### Modelling of atrial electrophysiology in fibrotic and non-fibrotic regions.

The methodology for computational modelling of the electrophysiology of the

atria of patients with PsAF and fibrotic remodelling can also be found in our published papers<sup>17,18,24,25,40,41</sup>. Specifically, at the cellular scale in non-fibrotic regions, a human chronic AF atrial action potential model<sup>42</sup> with modifications to fit clinical monophasic action potential recordings from patients with AF<sup>43</sup> was used to represent membrane kinetics in each atrial model. This ionic model results in an intrinsic action potential duration that is shorter than that of the normal human atrial action potential. At the tissue scale in the non-fibrotic myocardium, conductivity tensor values (longitudinal:  $\sigma_L = 0.126 \text{ S m}^{-1}$ ; transverse:  $\sigma_T = 0.0253 \text{ S m}^{-1}$ ) were calibrated to obtain an effective conduction velocity consistent with the range of values in patients with AF<sup>44</sup> ( $43.39 \text{ cm s}^{-1}$ ). Test simulations conducted in a regular grid with electrophysiological parameters calibrated using this method showed that longitudinal wavefront conduction in non-fibrotic tissue is in the convergent range (that is, negligible conduction velocity error between coarse and fine finite-element meshes with  $\sim 100$  and  $400 \mu\text{m}$  internode spacing, respectively).

In the fibrotic regions of the atria, changes to the action potential model were also implemented, as we have described previously<sup>17,18</sup> (+15.4% action potential duration; –49.6% upstroke velocity), representing the effect of elevated transforming growth factor- $\beta 1$ —a key component of the fibrogenic signalling pathway. These changes were achieved by reducing three of the underlying ionic currents<sup>45–50</sup> (–50% inward rectifier potassium; –50% L-type calcium; –40% fast sodium current). At the tissue scale, a reduction in conductivity values and a change in the anisotropy ratio ( $\sigma_L = 0.0547 \text{ S m}^{-1}$ ;  $\sigma_T = 0.00683 \text{ S m}^{-1}$ ) were used to represent interstitial fibrosis, gap junction remodelling and greater impairment of cell-to-cell coupling in the direction transverse to cardiac fibres<sup>51,52</sup>.

Analysis of retrospective patient-specific atrial simulations employing this modelling strategy has demonstrated good correlation with clinical results<sup>17,18,24,25,53</sup>. Systematic analysis of pre-ablation ECGI data<sup>53</sup> confirmed our earlier study's mechanistic prediction that RDs dynamically localize to the boundaries of fibrotic tissue clusters<sup>17</sup>. Moreover, using retrospective data from two cohorts of patients with PsAF at different medical centres, we showed that ablation targets predicted by simulations conducted blindly to the results of clinical mapping corresponded to the locations of AF-perpetuating RDs detected by either pre-procedural intracardiac mapping<sup>24</sup> or ECGI<sup>25</sup>.

While in this study we used a set of average human AF electrophysiological properties for non-fibrotic and fibrotic tissue, their distribution was patient specific. Nonetheless, the lack of full patient-specific electrophysiological properties could bring a level of uncertainty in identifying the OPTIMA targets. This was assessed in two sensitivity studies<sup>20,21</sup>, which demonstrated that the patient-specific distribution of fibrotic remodelling is the primary factor determining where RDs are anchored in the substrate. The electrophysiological properties determine RD cycle lengths, but this does not affect the locations of predicted targets. Nonetheless, changing electrophysiological properties resulted in RDs sometimes relocating to or appearing in other portions of the fibrotic substrate. However, our sensitivity analysis showed that this was mitigated in the OPTIMA workflow by iteratively performing virtual RD ablations until all possible ablation targets were identified. Thus, our approach unmasked all possible locations where RDs could potentially anchor, regardless of the electrophysiological properties.

**Simulation of electrical activity and numerical aspects.** The propagation of electrical activity in the personalized atria was simulated by solving the monodomain formulation for representing the spread of current in cardiac tissue using the finite-element method. This system was coupled with ordinary differential and algebraic equations representing myocyte membrane dynamics at each node in the mesh<sup>34</sup>. All simulations were executed using the CARP software package on a parallel computing system<sup>34,54</sup>. A version of this software that is free for academic use is available (<https://carp.medunigraz.at/carputils/>). Each simulation was run on one standard compute node, each of which was equipped with two Intel Broadwell dual socket, 14-core processors (2.6 GHz; 30 MB cache) and 128 GB of random-access memory. The compute time required to complete 1 s of simulation time depended on the size of the patient's heart, and ranged from  $\sim 20$  to  $\sim 80$  min across all patients (median (interquartile range): 43 min 3 s (37 min 52 s to 51 min 8 s)). The estimated total number of central processing unit hours for all simulations conducted in all models for this project was approximately 171 full days. Full details regarding the simulations of electrical activity in cardiac models can be found in our recent AF-related publications<sup>17,18</sup>, as well as earlier work by our team<sup>33,55,56</sup>.

**Atrial arrhythmia induction protocol.** As the flow chart of the OPTIMA approach (Fig. 1, top row) illustrates, each personalized 3D atrial electrophysiological model was used in simulations to determine all of the possible arrhythmias that could arise in the given fibrotic substrate. In each patient-derived model, arrhythmias were induced from 40 pacing sites distributed uniformly throughout the left and right atria, and the results of all 40 distinct simulations (conducted in parallel on a high-performance computing system, as described below) were analysed. The set of 40 pacing sites (see examples in Supplementary Fig. 4) was picked in each atrial model using an automatic approach that has been shown to reliably produce a desired interpoint spacing<sup>53</sup>. Pacing sites were placed

at least 2.5 mm away from the nearest region of dense fibrosis to ensure reliable capture. The distribution of pacing sites throughout the atria covered a large range of potential ectopic foci sites. Importantly, this distribution ensured that we captured all of the possible arrhythmias that could arise from the given patient-specific fibrotic substrate; this is an essential feature of the OPTIMA approach. For each pacing site, we ran a simulation that involved applying—at the specified location—a clinically relevant pacing sequence of 12 electrical stimuli with cycle lengths decreasing from 300 to 150 ms, to induce arrhythmias and thus assess the arrhythmogenic propensity of the fibrotic substrate. The protocol was identical to that in our previous publications<sup>17,18</sup>.

Notably, since there is no uniformly standardized pacing sequence for inducing AF in the clinic, this protocol is not intended to mimic stimulation that might be applied during an ablation procedure. Rather, it is a sequence that we have found useful for inducing RD-perpetuated AF episodes in atrial models constructed according to our methodology. Following the delivery of the final pacing stimulus, simulations were monitored for self-sustaining electrical wavefront propagation. For all cases in which activity persisted for 5,000 ms post-pacing, we applied further analysis to determine whether the cause was an induced RD or macroscopic re-entry.

**Analysis of pacing-induced atrial arrhythmias.** All pacing-induced arrhythmias were analysed to determine an initial set of ablation lesions (Fig. 1). The analysis consisted of determining the locations of the persistent RDs, as well as any possible macro re-entrant tachycardias. The atrial sites where the persistent RDs were localized were found by determining the RD phase singularity trajectories<sup>57</sup>. These were identified using the dynamic wavefront tip trajectory analysis approach<sup>20</sup>. Briefly, RD wavefront ‘pivot points’ were manually identified during a 1,000-ms analysis interval at the end of each simulation. This ensured that multiple RD rotations were analysed and that transient instability immediately following AF initiation was disregarded. In all cases, RDs persisted for at least two rotations and lasted at least 200 ms, which is consistent with the definition of RDs in previous publications<sup>14,58</sup>. While this facilitates a straightforward comparison between our study and a standardized clinical approach, in actual fact, most RDs observed in this study were spatiotemporally stable for the duration of the entire 1,000-ms analysis interval. Instances of macroscopic re-entry (that is, wavefront propagation around non-conductive obstacles such as the mitral or tricuspid valve annuli) were also identified (RD analysis was not applied in this case).

**Determining the OPTIMA ablation targets.** The bottom row of Fig. 1 illustrates the steps undertaken in finding the OPTIMA ablation targets. Based on the RD trajectories and macro re-entries identified in each atrial model, initial virtual ablation was performed in each model. Virtual ablation lesions consisted of the tissue volumes within 3.5 mm (that is, the ablation lesion radius for standard irrigated-tip catheters)<sup>32</sup> of each RD trajectory; the contained tissue volume was modelled as non-conductive, as in previous simulation studies<sup>18,59</sup>. If episodes of macro re-entrant atrial tachycardias or flutters were found, an ablation line transecting the narrowest part of the re-entrant pathway between non-conductive barriers was also included (see patient 9 in Fig. 2). The arrhythmia induction pacing protocol was then repeated to determine the emergence of new RDs or macro re-entries, which were then virtually ablated. This process was repeated iteratively until each model was rendered non-inducible for re-entrant atrial arrhythmias. To complete the personalized OPTIMA ablation target set, each predicted lesion (based on RD assessment) was connected to the nearest non-conductive anatomical feature (that is, boundaries of atrioventricular valves or left and right atrial veins) via linear lesions (see yellow lines in the rightmost column of Fig. 2), to avoid creating a new substrate for macro re-entrant atrial tachycardias or flutters.

**Importing personalized OPTIMA targets into the clinical electroanatomic navigation system.** The OPTIMA ablation target import process involved the following steps. First, the patient’s left atrial geometry was segmented from the MRA scan to construct a 3D surface mesh. Unlike LGE-MRI, the MRA surface shell provides visualization of the pulmonary veins, left atrial appendage and left lateral ridge, as needed for navigation during the procedure. Second, OPTIMA ablation targets in the left atrium were co-registered with the MRA surface shell. Third, since MRA scans do not provide accurate visualization of the right atrium, a downsampled right atrial surface shell was extracted from the LGE-MRI mesh with the OPTIMA targets. Fourth, the right atrial surface shell was co-registered, using affine transformation, with the left atrial MRA reference shell. Fifth, the left and right atrial surface shells with the OPTIMA targets were loaded into the CARTO navigation system and merged during the procedure, via the CARTOMERGE module, with a limited electroanatomic map (a 50-point shell) acquired by the mapping catheter, usually of the posterior wall. Multiple independent validation studies have shown that the registration error of the CARTOMERGE system is relatively small (~1–2 mm)<sup>60,61</sup>, and the benefit of merging patient-specific imaging with electroanatomic mapping data during conventional AF is well documented<sup>62,63</sup>, suggesting that locations displayed in the mapping system correlate well with the actual position of the catheter. In cases where this process failed, a CARTO technician manually annotated the locations of the OPTIMA targets onto the MRA shells.

**Ablation procedure.** Following the import of OPTIMA ablation targets into the electroanatomic navigation system, electrophysiology catheters were advanced under fluoroscopic guidance to the His bundle and coronary sinus in the right atrium with routine haemodynamic and electrocardiographic monitoring. An intracardiac echocardiography catheter was inserted into the right atrium and assisted in trans-septal puncture. A double trans-atrial septal puncture was performed under fluoroscopic guidance, and localization within the left atrium was confirmed with contrast as well as pressure tracing. Intravenous heparin was administered to achieve an activated clotting time of >350 s throughout the procedure. A 3.5-mm irrigated tip with a 2-mm interelectrode spacing ablation catheter (Thermocool Smarttouch; Biosense Webster) and a decapolar circular mapping catheter with a 25–15 loop diameter and 8 mm interelectrode spacing (LASSO 2515 Variable Loop Eco Nav; Biosense Webster) were advanced under fluoroscopic guidance to the left atrium. Pulmonary venous angiograms were then obtained for each of the four pulmonary veins. Using a circular Lasso catheter, pulmonary vein electrograms were measured at baseline. In patients undergoing repeat AF ablation, pulmonary vein–left atrium electrical reconnections were noted. The limited electroanatomic map of the left atrium mentioned above, created with the Smarttouch catheter, was registered to the previously segmented left atrial MRA shell (including OPTIMA target annotations) using standard landmark-based methods followed by surface registration techniques. High-output pacing was performed along the anterior aspect of the right pulmonary veins to confirm the absence of phrenic nerve capture. The oesophagus was marked with a radio-opaque temperature probe for monitoring during ablation. Following OPTIMA-guided ablation, PVI (the standard of care) was performed in all patients.

Before the procedure, videos displaying OPTIMA targets with the nearby anatomical landmarks annotated were made available to physicians for review and planning. For consistency with previous studies of targeted RD ablation<sup>22</sup>, in cases where patients presented in sinus rhythm, AF was induced with burst pacing and stabilized for at least 10 min before OPTIMA target ablation. Radiofrequency ablation of OPTIMA targets was performed with the Smarttouch irrigated catheter at the annotated targets using a power of 25 W on the posterior wall and 30 W elsewhere. OPTIMA targets were ablated sequentially, beginning with those corresponding to locations where RDs were induced by a larger number of pacing distinct sites in simulations conducted in the corresponding patient-specific model. Ablation of OPTIMA targets was continued, even in cases where acute AF termination was achieved during the procedure, since the specific purpose of OPTIMA ablation was to eliminate the propensity of the fibrotic substrate to sustain arrhythmias. Energy was applied for 15–30 s at each target. No immediate postoperative complications were reported.

**Patient follow-up.** Patient rhythm follow-up consisted of electrocardiograms and clinical evaluation every 3 months, with ambulatory event monitors as indicated by symptoms.

**Statistics.** The results are presented as means  $\pm$  s.d. for variables that are expected to be normally distributed (for example, patient age, procedure times, the extent of atrial fibrosis, and so on). For other variables, medians and interquartile ranges are used as summary statistics instead. Categorical variables are expressed as percentages.

**Reporting Summary.** Further information on research design is available in the Nature Research Reporting Summary linked to this article.

## Code availability

The image-processing software ITK-SNAP is freely available from <http://www.itksnap.org/>. Computational meshes were generated using the commercial software Simpleware ScanIP (Synopsys). Source code for the human atrial ionic model is freely available from the repository CellML (<https://models.physiomeproject.org/exposure/0e03bbe01606be5811691f9d5de10b65>). All simulations were conducted using the software package CARP, a free version of which can be downloaded for academic use via <https://carp.medunigraz.at/carputils/>. Simulation results were visualized using either Meshalyzer (which can be downloaded via <https://github.com/cardiosolv/meshalyzer>) or ParaView (Kitware) (which can be downloaded via <https://www.paraview.org/download/>). Data from clinical procedures were visualized using the commercial software CARTOMERGE (Biosense Webster).

## Data availability

Relevant data, including patient MRI scans, are available from the authors on approval from the Johns Hopkins Institutional Review Board.

Received: 31 August 2018; Accepted: 3 July 2019;  
Published online: 19 August 2019

## References

- Andrade, J., Khairy, P., Dobrev, D. & Nattel, S. The clinical profile and pathophysiology of atrial fibrillation: relationships among clinical features, epidemiology, and mechanisms. *Circ. Res.* **114**, 1453–1468 (2014).



2. Go, A. S. et al. Prevalence of diagnosed atrial fibrillation in adults: national implications for rhythm management and stroke prevention: the AnTicoagulation and Risk Factors in Atrial Fibrillation (ATRIA) Study. *J. Am. Med. Assoc.* **285**, 2370–2375 (2001).
3. Dorian, P. et al. The impairment of health-related quality of life in patients with intermittent atrial fibrillation: implications for the assessment of investigational therapy. *J. Am. Coll. Cardiol.* **36**, 1303–1309 (2000).
4. Kalantarian, S., Stern, T. A., Mansour, M. & Ruskin, J. N. Cognitive impairment associated with atrial fibrillation: a meta-analysis. *Ann. Intern. Med.* **158**, 338–346 (2013).
5. Stewart, S., Murphy, N. F., Walker, A., McGuire, A. & McMurray, J. J. Cost of an emerging epidemic: an economic analysis of atrial fibrillation in the UK. *Heart* **90**, 286–292 (2004).
6. Calkins, H. et al. 2017 HRS/EHRA/ECAS/APHRS/SOLAECE expert consensus statement on catheter and surgical ablation of atrial fibrillation. *Heart Rhythm* **14**, e275–e444 (2017).
7. Oakes, R. S. et al. Detection and quantification of left atrial structural remodeling with delayed-enhancement magnetic resonance imaging in patients with atrial fibrillation. *Circulation* **119**, 1758–1767 (2009).
8. Marrouche, N. F. et al. Association of atrial tissue fibrosis identified by delayed enhancement MRI and atrial fibrillation catheter ablation: the DECAAF study. *J. Am. Med. Assoc.* **311**, 498–506 (2014).
9. Scherr, D. et al. Five-year outcome of catheter ablation of persistent atrial fibrillation using termination of atrial fibrillation as a procedural endpoint. *Circ. Arrhythm. Electrophysiol.* **8**, 18–24 (2015).
10. Xu, J. et al. Atrial extracellular matrix remodeling and the maintenance of atrial fibrillation. *Circulation* **109**, 363–368 (2004).
11. Tanaka, K. et al. Spatial distribution of fibrosis governs fibrillation wave dynamics in the posterior left atrium during heart failure. *Circ. Res.* **101**, 839–847 (2007).
12. Verma, A. et al. Approaches to catheter ablation for persistent atrial fibrillation. *N. Engl. J. Med.* **372**, 1812–1822 (2015).
13. Rappel, W. J., Zaman, J. A. & Narayan, S. M. Mechanisms for the termination of atrial fibrillation by localized ablation: computational and clinical studies. *Circ. Arrhythm. Electrophysiol.* **8**, 1325–1333 (2015).
14. Haissaguerre, M. et al. Driver domains in persistent atrial fibrillation. *Circulation* **130**, 530–538 (2014).
15. Swarup, V. et al. Stability of rotors and focal sources for human atrial fibrillation: focal impulse and rotor mapping (FIRM) of AF sources and fibrillatory conduction. *J. Cardiovasc. Electrophysiol.* **25**, 1284–1292 (2014).
16. Trayanova, N. A. Mathematical approaches to understanding and imaging atrial fibrillation: significance for mechanisms and management. *Circ. Res.* **114**, 1516–1531 (2014).
17. Zahid, S. et al. Patient-derived models link re-entrant driver localization in atrial fibrillation to fibrosis spatial pattern. *Cardiovasc. Res.* **110**, 443–454 (2016).
18. Zahid, S. et al. Feasibility of using patient-specific models and the “minimum cut” algorithm to predict optimal ablation targets for left atrial flutter. *Heart Rhythm* **13**, 1687–1698 (2016).
19. Shim, J. et al. Virtual in-silico modeling guided catheter ablation predicts effective linear ablation lesion set for longstanding persistent atrial fibrillation: multicenter prospective randomized study. *Front. Physiol.* **8**, 792 (2017).
20. Deng, D. et al. Sensitivity of reentrant driver localization to electrophysiological parameter variability in image-based computational models of persistent atrial fibrillation sustained by a fibrotic substrate. *Chaos* **27**, 093932 (2017).
21. Hakim, J. B., Murphy, M. J., Trayanova, N. A. & Boyle, P. M. Arrhythmia dynamics in computational models of the atria following virtual ablation of re-entrant drivers. *Europace* **20**, iii45–iii54 (2018).
22. Narayan, S. M. et al. Treatment of atrial fibrillation by the ablation of localized sources: CONFIRM (Conventional Ablation for Atrial Fibrillation With or Without Focal Impulse and Rotor Modulation) trial. *J. Am. Coll. Cardiol.* **60**, 628–636 (2012).
23. Ramanathan, C., Ghanem, R. N., Jia, P., Ryu, K. & Rudy, Y. Noninvasive electrocardiographic imaging for cardiac electrophysiology and arrhythmia. *Nat. Med.* **10**, 422–428 (2004).
24. Boyle, P. M. et al. The fibrotic substrate in persistent atrial fibrillation patients: comparison between predictions from computational modeling and measurements from focal impulse and rotor mapping. *Front. Physiol.* **9**, 1151 (2018).
25. Boyle, P. M. et al. Comparing reentrant drivers predicted by image-based computational modeling and mapped by electrocardiographic imaging in persistent atrial fibrillation. *Front. Physiol.* **9**, 414 (2018).
26. Lalani, G. G. et al. Organized sources are spatially conserved in recurrent compared to pre-ablation atrial fibrillation: further evidence for non-random electrical substrates. *J. Cardiovasc. Electrophysiol.* **27**, 661–669 (2016).
27. Brooks, A. G. et al. Outcomes of long-standing persistent atrial fibrillation ablation: a systematic review. *Heart Rhythm* **7**, 835–846 (2010).
28. McGann, C. et al. Atrial fibrillation ablation outcome is predicted by left atrial remodeling on MRI. *Circ. Arrhythm. Electrophysiol.* **7**, 23–30 (2014).
29. Khurram, I. M. et al. Magnetic resonance image intensity ratio, a normalized measure to enable interpatient comparability of left atrial fibrosis. *Heart Rhythm* **11**, 85–92 (2014).
30. Yushkevich, P. A. et al. User-guided 3D active contour segmentation of anatomical structures: significantly improved efficiency and reliability. *NeuroImage* **31**, 1116–1128 (2006).
31. Karim, R. et al. Evaluation of state-of-the-art segmentation algorithms for left ventricle infarct from late gadolinium enhancement MR images. *Med. Image Anal.* **30**, 95–107 (2016).
32. Raya, S. P. & Udupa, J. K. Shape-based interpolation of multidimensional objects. *IEEE Trans. Med. Imaging* **9**, 32–42 (1990).
33. Vadakkumpadan, F. et al. Image-based models of cardiac structure with applications in arrhythmia and defibrillation studies. *J. Electro.* **42**, 157.e1–157.e10 (2009).
34. Plank, G. et al. From mitochondrial ion channels to arrhythmias in the heart: computational techniques to bridge the spatio-temporal scales. *Phil. Trans. A Math. Phys. Eng. Sci.* **366**, 3381–3409 (2008).
35. Niederer, S. A. et al. Verification of cardiac tissue electrophysiology simulators using an N-version benchmark. *Phil. Trans. A Math. Phys. Eng. Sci.* **369**, 4331–4351 (2011).
36. Beg, M. F., Helm, P. A., McVeigh, E., Miller, M. I. & Winslow, R. L. Computational cardiac anatomy using MRI. *Magn. Reson. Med.* **52**, 1167–1174 (2004).
37. McDowell, K. S. et al. Methodology for patient-specific modeling of atrial fibrosis as a substrate for atrial fibrillation. *J. Electrocardiol.* **45**, 640–645 (2012).
38. McDowell, K. S. et al. Mechanistic inquiry into the role of tissue remodeling in fibrotic lesions in human atrial fibrillation. *Biophys. J.* **104**, 2764–2773 (2013).
39. Labarthe, S. et al. A bilayer model of human atria: mathematical background, construction, and assessment. *Europace* **16**, iv21–iv29 (2014).
40. Roney, C. H. et al. Modelling methodology of atrial fibrosis affects rotor dynamics and electrograms. *Europace* **18**, iv146–iv155 (2016).
41. Boyle, P. M., Zahid, S. & Trayanova, N. A. Towards personalized computational modelling of the fibrotic substrate for atrial arrhythmia. *Europace* **18**, iv136–iv145 (2016).
42. Courtemanche, M., Ramirez, R. J. & Nattel, S. Ionic mechanisms underlying human atrial action potential properties: insights from a mathematical model. *Am. J. Physiol.* **275**, H301–H321 (1998).
43. Krummen, D. E. et al. Mechanisms of human atrial fibrillation initiation: clinical and computational studies of repolarization restitution and activation latency. *Circ. Arrhythm. Electrophysiol.* **5**, 1149–1159 (2012).
44. Konings, K. T. et al. High-density mapping of electrically induced atrial fibrillation in humans. *Circulation* **89**, 1665–1680 (1994).
45. Avila, G., Medina, I. M., Jimenez, E., Elizondo, G. & Aguilar, C. I. Transforming growth factor- $\beta$ 1 decreases cardiac muscle L-type  $\text{Ca}^{2+}$  current and charge movement by acting on the  $\text{Ca}_v1.2$  mRNA. *Am. J. Physiol. Heart Circ. Physiol.* **292**, H622–H631 (2007).
46. Nattel, S., Burstein, B. & Dobrev, D. Atrial remodeling and atrial fibrillation: mechanisms and implications. *Circ. Arrhythm. Electrophysiol.* **1**, 62–73 (2008).
47. Corradi, D., Callegari, S., Maestri, R., Benussi, S. & Alfieri, O. Structural remodeling in atrial fibrillation. *Nat. Clin. Pract. Cardiovasc. Med.* **5**, 782–796 (2008).
48. Pedrotty, D. M., Klinger, R. Y., Kirkton, R. D. & Bursac, N. Cardiac fibroblast paracrine factors alter impulse conduction and ion channel expression of neonatal rat cardiomyocytes. *Cardiovasc. Res.* **83**, 688–697 (2009).
49. Kakkar, R. & Lee, R. T. Intramyocardial fibroblast myocyte communication. *Circ. Res.* **106**, 47–57 (2010).
50. Ramos-Mondragon, R., Vega, A. V. & Avila, G. Long-term modulation of  $\text{Na}^+$  and  $\text{K}^+$  channels by TGF- $\beta$ 1 in neonatal rat cardiac myocytes. *Pflug. Arch.* **461**, 235–247 (2011).
51. Li, D., Fareh, S., Leung, T. K. & Nattel, S. Promotion of atrial fibrillation by heart failure in dogs: atrial remodeling of a different sort. *Circulation* **100**, 87–95 (1999).
52. Burstein, B. et al. Changes in connexin expression and the atrial fibrillation substrate in congestive heart failure. *Circ. Res.* **105**, 1213–1222 (2009).
53. Cochet, H. et al. Relationship between fibrosis detected on late gadolinium-enhanced cardiac magnetic resonance and re-entrant activity assessed with electrocardiographic imaging in human persistent atrial fibrillation. *JACC Clin. Electrophysiol.* **4**, 17–29 (2018).
54. Vigmond, E. J., Weber Dos Santos, R., Prassl, A. J., Deo, M. & Plank, G. Solvers for the cardiac bidomain equations. *Prog. Biophys. Mol. Biol.* **96**, 3–18 (2008).
55. Boyle, P. M., Williams, J. C., Ambrosi, C. M., Entcheva, E. & Trayanova, N. A. A comprehensive multiscale framework for simulating optogenetics in the heart. *Nat. Commun.* **4**, 2370 (2013).
56. Arevalo, H. J. et al. Arrhythmia risk stratification of patients after myocardial infarction using personalized heart models. *Nat. Commun.* **7**, 11437 (2016).
57. Eason, J. & Trayanova, N. Phase singularities and termination of spiral wave reentry. *J. Cardiovasc. Electrophysiol.* **13**, 672–679 (2002).

58. Narayan, S. M., Krummen, D. E. & Rappel, W. J. Clinical mapping approach to diagnose electrical rotors and focal impulse sources for human atrial fibrillation. *J. Cardiovasc. Electrophysiol.* **23**, 447–454 (2012).
59. Arevalo, H., Plank, G., Helm, P., Halperin, H. & Trayanova, N. Tachycardia in post-infarction hearts: insights from 3D image-based ventricular models. *PLoS ONE* **8**, e68872 (2013).
60. Tops, L. F. et al. Fusion of multislice computed tomography imaging with three-dimensional electroanatomic mapping to guide radiofrequency catheter ablation procedures. *Heart Rhythm* **2**, 1076–1081 (2005).
61. Dong, J. et al. Impact of heart rhythm status on registration accuracy of the left atrium for catheter ablation of atrial fibrillation. *J. Cardiovasc. Electrophysiol.* **18**, 1269–1276 (2007).
62. Martinek, M., Nesser, H. J., Aichinger, J., Boehm, G. & Purerfellner, H. Impact of integration of multislice computed tomography imaging into three-dimensional electroanatomic mapping on clinical outcomes, safety, and efficacy using radiofrequency ablation for atrial fibrillation. *Pacing Clin. Electrophysiol.* **30**, 1215–1223 (2007).
63. Bertaglia, E. et al. Image integration increases efficacy of paroxysmal atrial fibrillation catheter ablation: results from the CartoMerge Italian Registry. *Europace* **11**, 1004–1010 (2009).

## Acknowledgements

This project was supported by grants from the NIH (DP1-HL123271 to N.A.T. and U01-HL141074 to N.A.T. and P.M.B.), the AHA (16-SDG-30440006 to P.M.B.), Biosense Webster (to S.N.) and the NSF (graduate fellowship to S.Z.). This project has received funding from the Leducq Foundation (Research Grant number 16 CVD 02). This project was also supported by the Roz and Marvin H. Weiner and Family Foundation, the

Dr Francis P. Chiamonte Private Foundation, M. Poindexter, C. Poindexter and the Norbert and Louise Grunwald Cardiac Arrhythmia Research Fund.

## Author contributions

T.Z., P.M.B., S.Z., A.P., S.N., H.C. and N.A.T. designed the study. P.M.B., S.Z., R.L.A., D.D., W.H.F., J.B.H. and M.J.M. conducted the simulations and analysed the simulation results. T.Z., P.M.B., S.Z., R.L.A., J.B.H., A.P., S.L.Z., H.A., J.E.M., A.K., S.N., D.D.S., H.C. and N.A.T. interpreted the imaging and simulation data. H.A., J.E.M. and H.C. performed the catheter ablation procedures. T.Z., P.M.B. and N.A.T. wrote the paper. H.A., J.E.M., D.D.S. and H.C. edited the manuscript.

## Competing interests

N.A.T. has filed a patent application (US patent application number US0161100A1; World Intellectual Property Organization application number WO2015/084876A1; European Patent Office application number EP3076869A4; Japan application number JP2016540570A; Israel application number IL245988D0; entitled 'Systems and methods for atrial fibrillation treatment and risk assessment') that is currently under review.

## Additional information

**Supplementary information** is available for this paper at <https://doi.org/10.1038/s41551-019-0437-9>.

**Reprints and permissions information** is available at [www.nature.com/reprints](http://www.nature.com/reprints).

**Correspondence and requests for materials** should be addressed to N.A.T.

**Publisher's note:** Springer Nature remains neutral with regard to jurisdictional claims in published maps and institutional affiliations.

© The Author(s), under exclusive licence to Springer Nature Limited 2019

## Reporting Summary

Nature Research wishes to improve the reproducibility of the work that we publish. This form provides structure for consistency and transparency in reporting. For further information on Nature Research policies, see [Authors & Referees](#) and the [Editorial Policy Checklist](#).

### Statistical parameters

When statistical analyses are reported, confirm that the following items are present in the relevant location (e.g. figure legend, table legend, main text, or Methods section).

n/a Confirmed

- ☒ ☐ The exact sample size (*n*) for each experimental group/condition, given as a discrete number and unit of measurement
- ☒ ☐ An indication of whether measurements were taken from distinct samples or whether the same sample was measured repeatedly
- ☒ ☐ The statistical test(s) used AND whether they are one- or two-sided  
*Only common tests should be described solely by name; describe more complex techniques in the Methods section.*
- ☒ ☐ A description of all covariates tested
- ☒ ☐ A description of any assumptions or corrections, such as tests of normality and adjustment for multiple comparisons
- ☒ ☐ A full description of the statistics including central tendency (e.g. means) or other basic estimates (e.g. regression coefficient) AND variation (e.g. standard deviation) or associated estimates of uncertainty (e.g. confidence intervals)
- ☒ ☐ For null hypothesis testing, the test statistic (e.g. *F*, *t*, *r*) with confidence intervals, effect sizes, degrees of freedom and *P* value noted  
*Give P values as exact values whenever suitable.*
- ☒ ☐ For Bayesian analysis, information on the choice of priors and Markov chain Monte Carlo settings
- ☒ ☐ For hierarchical and complex designs, identification of the appropriate level for tests and full reporting of outcomes
- ☒ ☐ Estimates of effect sizes (e.g. Cohen's *d*, Pearson's *r*), indicating how they were calculated
- ☒ ☐ Clearly defined error bars  
*State explicitly what error bars represent (e.g. SD, SE, CI)*

Our web collection on [statistics for biologists](#) may be useful.

### Software and code

Policy information about [availability of computer code](#)

Data collection

No software was used in the data collection component of this study.

Data analysis

Relevant data, including patient MRI scans, are available from the authors upon approval of Johns Hopkins Institutional Review Board. The image processing software ITK-Snap is freely available from <http://www.itksnap.org/>. Computational meshes are generated using the commercial software Simpleware ScanIP (Synopsis, Inc.). Source code for the human atrial ionic model by is freely available from the repository CellML (<https://models.physiomeproject.org/exposure/0e03bbe01606be5811691f9d5de10b65>). All simulations are conducted using the software package CARP, a free version of which can be downloaded for academic use via <https://carp.medunigraz.at/carputils/>. Simulation results were visualized using meshalyzer, which can be downloaded via <https://github.com/cardiosolv/meshalyzer> or Paraview (Kitware), which can be downloaded via <https://www.paraview.org/download/>. Data from clinical procedures were visualized using the commercial software CARTOMERGE™ (Biosense Webster).

For manuscripts utilizing custom algorithms or software that are central to the research but not yet described in published literature, software must be made available to editors/reviewers upon request. We strongly encourage code deposition in a community repository (e.g. GitHub). See the Nature Research [guidelines for submitting code & software](#) for further information.



## Data

Policy information about [availability of data](#)

All manuscripts must include a [data availability statement](#). This statement should provide the following information, where applicable:

- Accession codes, unique identifiers, or web links for publicly available datasets
- A list of figures that have associated raw data
- A description of any restrictions on data availability

Relevant data, including patient MRI scans, are available from the authors upon approval of Johns Hopkins Institutional Review Board.

## Field-specific reporting

Please select the best fit for your research. If you are not sure, read the appropriate sections before making your selection.

☒ Life sciences ☐ Behavioural & social sciences ☐ Ecological, evolutionary & environmental sciences

For a reference copy of the document with all sections, see [nature.com/authors/policies/ReportingSummary-flat.pdf](https://www.nature.com/authors/policies/ReportingSummary-flat.pdf)

## Life sciences study design

All studies must disclose on these points even when the disclosure is negative.

Sample size	The number of subjects in the study was limited ,as this is feasibility study to demonstrate the utility of a novel technology. From May '16 to July '17, 10 eligible patients were enrolled (persistent atrial fibrillation catheter ablation candidate, not enrolled in other conflicting clinical trials, meeting inclusion criteria outlined in Methods) at Johns Hopkins Hospital.
Data exclusions	No relevant data were excluded from this study.
Replication	The numerical stability and reproducibility of the software CARP has been thoroughly tested by our group. Since all models are deterministic, simulation results would be the same when repeated.
Randomization	n/a - This is a technology feasibility study, not a randomized clinical trial
Blinding	The team performing the simulations were only given the patient MRI scans. No other clinical information was available until after the OPTIMA analysis was complete.

## Reporting for specific materials, systems and methods

### Materials & experimental systems

n/a	Involved in the study
<input checked="" type="checkbox"/>	<input type="checkbox"/> Unique biological materials
<input checked="" type="checkbox"/>	<input type="checkbox"/> Antibodies
<input checked="" type="checkbox"/>	<input type="checkbox"/> Eukaryotic cell lines
<input checked="" type="checkbox"/>	<input type="checkbox"/> Palaeontology
<input checked="" type="checkbox"/>	<input type="checkbox"/> Animals and other organisms
<input type="checkbox"/>	<input checked="" type="checkbox"/> Human research participants

### Methods

n/a	Involved in the study
<input checked="" type="checkbox"/>	<input type="checkbox"/> ChIP-seq
<input checked="" type="checkbox"/>	<input type="checkbox"/> Flow cytometry
<input checked="" type="checkbox"/>	<input type="checkbox"/> MRI-based neuroimaging

## Human research participants

Policy information about [studies involving human research participants](#)

Population characteristics	All patients had symptomatic, drug-refractory PsAF and presented to Johns Hopkins Hospital for catheter ablation. All patients had LGE-MRI scans of sufficient quality to reconstruct a personalized computational model of the left and right atria.
Recruitment	Exclusion criteria are outlined in Methods. Compared to other similar studies of persistent AF ablation, we excluded very few patients. For example, we included 6/10 individuals with previous failed ablations (up to 3 prior failed procedures). As such, there is no selection bias towards patients in whom a positive response to therapy might have been more likely.